Published on 18 November 2014. Downloaded by University of Science and Technology of China on 10/03/2016 03:24:25.

ChemComm

COMMUNICATION

View Article Online
View Journal | View Issue

Cite this: *Chem. Commun.*, 2015, 51, 866

Received 8th October 2014,
Accepted 17th November 2014

DOI: 10.1039/c4cc07937j

www.rsc.org/chemcomm

Highly sensitive surface-enhanced Raman scattering based on multi-dimensional plasmonic coupling in Au–graphene–Ag hybrids†

Yuan Zhao,[a] Wencong Zeng,[a] Zhuchen Tao,[a] Penghui Xiong,[b] Yan Qu[cd] and Yanwu Zhu*[ae]

We report an efficient surface-enhanced Raman scattering (SERS) substrate by utilizing the multi-dimensional plasmonic coupling in Au nanoparticle (NP)–graphene–Ag NP hybrid structures. An ultrasensitive SERS detection with a limit of down to 10^{-13} M has been achieved when the sandwiched hybrid film is fabricated on an Ag substrate.

Surface-enhanced Raman scattering (SERS) has attracted increasing attention in diverse areas, including chemistry, biology, food safety and biomedical diagnostics since the first observation reported on a rough silver electrode in 1974.[1–3] Until now, metallic nanostructures with various morphologies and interparticle spaces, such as nanocubes,[4] nanospheres,[5] nano-octahedrons,[6] nanostars,[7] nanowires[8] and nano-pyramids,[9] have been explored to enhance the Raman signals since the hot spots depend strongly on the shape of metal nanoparticles (NPs) and the interparticle distance. Among the metals used, silver (Ag) has been demonstrated to have a greater enhancement factor (EF) than gold (Au) due to the absence of interband absorption,[10–12] but the bad chemical stability and biocompatibility restrict the long-term employment of Ag-based SERS substrates. Many strategies, *e.g.* by developing Ag–Au,[13,14] Ag–SiO_2[15] and Ag–TiO_2[16] core–shell nanostructures, have been proposed in order to sheath Ag NPs for improved stability. However, the accurate control of the reaction conditions to obtain uniform NPs and reproducible Raman signals remains a challenge.[10,17] Moreover, a certain thickness of the shell layer is necessary for a complete coverage of Ag,[18] but may severely depress the Raman signal as the electric field enhancement is a highly localized effect and decays exponentially away from the Ag surface.[19] In addition, it is difficult to tune the plasmonic resonant wavelength of such core–shell NPs through the fabrication, leading to limited Raman sensitivity.[20,21]

Graphene has been intensively studied and been found to play an important role in SERS.[9,22–25] For example, an EF of 2–17 has been obtained from mechanically cleaved graphene for detecting aromatic molecules.[26] This enhancement has been attributed to the chemical enhancement since the surface plasmon of graphene is in the mid-infrared or terahertz regions.[26] In the visible and near-infrared regions, on the other hand, graphene acts as a dielectric.[27] Thus graphene–metal NP structures have been designed to enhance Raman sensitivity. For example, graphene-covered metallic nanostructures[9,28] and NPs residing on graphene[25,29,30] have been proposed with improved Raman activity. Although graphene oxide (GO)/reduced graphene oxide (rGO) embedded hybrid structures could also enhance Raman signals, the considerable difficulty in controlling the reaction conditions makes it difficult to obtain uniform and well-defined thickness of GO/rGO or the reduction degree of rGO.[10,18,31,32] In our previous work, we have developed a simple technique to achieve sub-nanometer gaps between two layers of Au NPs by constructing Au NP–graphene–Au NP sandwich hybrids; the Raman signals of graphene and biomolecules on such a hybrid substrate have been enhanced due to the coupling of NP–NP and NP–graphene.[33] However, owing to the mismatch of the plasmonic resonant wavelength with the excitation laser wavelength and the relatively weaker Raman activity of Au than Ag (resulting from the absence of interband absorption of Ag), the SERS sensitivity could not be optimized by simply tuning the particle sizes of Au in our previous work. As far as we know, there have been no comprehensive experimental schemes that take into account the optical tunability, chemical stability and Raman sensitivity when two different metals, *e.g.* Au and Ag, are involved in a chemical vapor deposition (CVD) grown graphene–plasmonic hybrid system.

Herein, we propose an efficient SERS substrate by utilizing the multi-dimensional plasmonic coupling in Au NP–graphene–Ag NP structures. It is found that the plasmonic resonant wavelength and

[a] *Department of Materials Science and Engineering & CAS Key Laboratory of Materials for Energy Conversion, University of Science and Technology of China, Hefei 230026, China. E-mail: zhuyanwu@ustc.edu.cn*
[b] *Department of Precision Machinery and Precision Instrumentation, University of Science and Technology of China, Hefei, 230026, China*
[c] *Wuxi Graphene Technologies Co., Ltd, 311 Yanxin Rd, Wuxi 214174, China*
[d] *China Jiangnan Graphene Research Institute, 6 Xiangyun Rd, Changzhou 213149, China*
[e] *Collaborative Innovation Center of Chemistry for Energy Materials (2011-iChEM), Hefei 230026, China*

† Electronic supplementary information (ESI) available: Experimental details and additional figures. See DOI: 10.1039/c4cc07937j

This journal is © The Royal Society of Chemistry 2015

Published on 18 November 2014. Downloaded by University of Science and Technology of China on 10/03/2016 03:24:25.

magnitude of the hybrid platform can be readily tuned by the thickness of both Au and Ag films deposited. In this way, a resonant wavelength equal to the excitation laser wavelength (532 nm) is achieved using an 8 nm Au/monolayer graphene (1LG)/8 nm Ag hybrid film. Finite element simulations reveal that both the coupling between the same type of metal NPs and that between vertical Au/Ag NPs contribute to the electric field enhancement. Based on the multi-dimensional coupling in the hybrid films, we demonstrate that as-fabricated 8 nm Au/1LG/8 nm Ag structures show a dramatic enhancement in Raman signals when detecting aromatic molecules such as rhodamine B (RhB) and rhodamine 6G (R6G) and explosive trinitrotoluene (TNT).

The fabrication procedure of Au NP–graphene–Ag NP hybrid films is schematically illustrated in Fig. 1a. Ag films were firstly deposited onto a freshly cleaned quartz substrate by plasma sputtering.[34] Ag NPs were obtained by annealing the deposited Ag film at 300 °C for 100 min with 100 sccm flowing Ar in a quartz tube furnace (step 1). Monolayer graphene films grown on Cu foils by CVD were then wet-transferred onto the surface of Ag NPs using poly(methyl methacrylate) (PMMA) as a transfer reagent,[35] forming a graphene-covered Ag NP structure (step 2). Au NP–graphene–Ag NP sandwiched films were obtained after another Au film was deposited and annealed (step 3). Fig. 1b–g show the SEM and AFM images of the samples sequentially obtained from the steps mentioned above. Fig. 1b is the SEM image of the 1LG-covered Ag NP structure obtained by depositing and annealing an 8 nm-thick Ag film, showing both the bare Ag NPs and graphene-covered regions. For convenience, in the following discussion we shall name the Ag NPs obtained by annealing 8 nm-thick Ag film as '8 nm Ag' and the Au NPs obtained by annealing 8 nm-thick Au film as '8 nm Au'. The topography for 8 nm Ag and 1LG-covered 8 nm Ag was tracked by AFM and is shown in Fig. 1d and e. The size distribution of 8 nm Ag is shown in Fig. S1, ESI.† The surface of graphene covered Ag NPs shows a smaller roughness (arithmetic average deviation) of 6.5 nm compared with that of bare Ag NPs (13.6 nm). Fig. 1c shows the SEM image of the exactly same area shown in Fig. 1b after the 8 nm-thick Au film was deposited and annealed. In contrast to the sandwiched structure with graphene embedded (Fig. 1g), the 8 nm Au/8 nm Ag direct stacking without graphene embedded aggregates to a single layer of NPs with a larger particle density, as shown in Fig. 1f. The Raman spectra further evidence the uniform coverage of graphene in graphene-covered 8 nm Ag and 8 nm Au/1LG/8 nm Ag structures (Fig. S2, ESI†). Our previous work has shown that the electrons in Au NPs are reluctant to interact with neighboring graphene;[36] thus the graphene layer here serves as a good medium to define an ideal sub-nanometer gap for enhancing the coupling between plasmonic Au/Ag NPs.

The optical properties of bare Ag, bare Au, Au/Ag and Au/1LG/Ag hybrid films have been investigated as a function of the thickness of metals, as shown in Fig. S3 and S4, ESI.† As can be seen, the proposed hybrid film has an advantage of a tunable resonant wavelength, which allows us to fabricate a structure with a resonant wavelength close or equal to the excitation laser wavelength, in order to maximize the SERS sensitivity.[20] Such a tunability is not easy to be realized by simply tuning the thickness of bare Ag or bare Au films.[20,22,37] Thus the 8 nm Au/1LG/8 nm Ag hybrid film was prepared to match the laser wavelength of 532 nm used in our measurements. In contrast, the weak Raman sensitivity from bare metal NPs compared to Au NP–graphene–Ag NP hybrids may be related to the weak light absorption (see ESI†).[36,38,39] Fig. 2a shows the curves of optical absorption *versus* wavelength for 8 nm Au, 8 nm Ag, 8 nm Au/8 nm Ag and 8 nm Au/1LG/8 nm Ag, respectively.

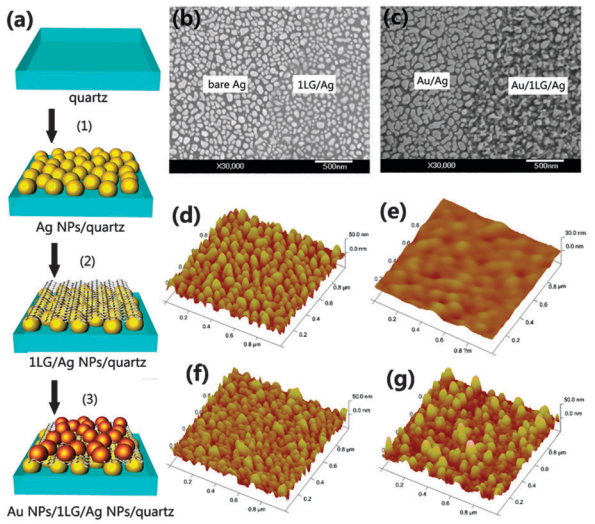

Fig. 1 (a) Schematic illustration of the sample preparation process for the Au NP–graphene–Ag NP hybrid structures. (b) SEM image of 1LG-covered 8 nm Ag, showing both bare Ag and graphene-covered regions. (c) SEM image of the same area shown in (b) after an 8 nm-thick Au film was deposited and annealed. AFM images of (d) 8 nm Ag, (e) 1LG-covered 8 nm Ag, (f) 8 nm Au/8 nm Ag and (g) 8 nm Au/1LG/8 nm Ag films, respectively.

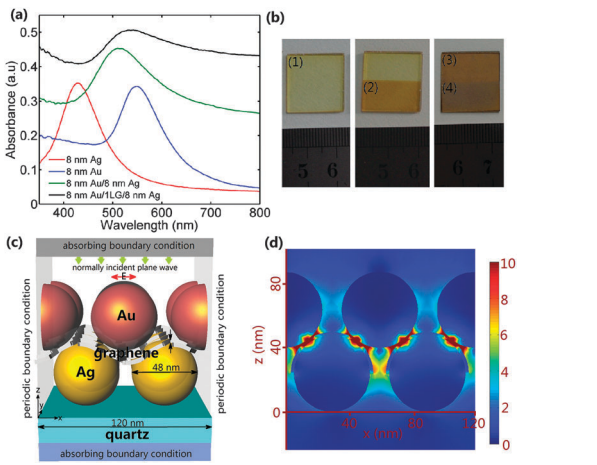

Fig. 2 (a) Absorption spectra of 8 nm Ag, 8 nm Au, 8 nm Au/8 nm Ag and 8 nm Au/1LG/8 nm Ag films on quartz substrates. (b) Optical images of 8 nm Ag (region 1), 1LG-covered 8 nm Ag (region 2), 8 nm Au/8 nm Ag (region 3) and 8 nm Au/1LG/8 nm Ag (region 4). (c) Simulation configuration of Au NP–graphene–Ag NP on a quartz substrate. The lateral period is 120 nm; the diameter of both Au and Ag NPs is 48 nm; 1LG veiling on Ag NPs has a thickness of 1 nm. A plane lightwave with a polarized electric field along the *x* direction was launched normally from the top. (d) Simulated electrical field intensity distributions of Au NP–graphene–Ag NP on a quartz substrate in the *xz* plane with y = 24 nm. The color bar demonstrates the magnitude of the electric field normalized by the incident field.

Published on 18 November 2014. Downloaded by University of Science and Technology of China on 10/03/2016 03:24:25.

As we can see, the resonant wavelength is located at 429 nm or 548 nm for pure 8 nm Ag or 8 nm Au, respectively; while the peak from the hybrid films is located in between, *e.g.* at 517 nm for 8 nm Au/8 nm Ag or at 532 nm for 8 nm Au/1LG/8 nm Ag. Correspondingly the optical images in Fig. 2b demonstrate that the color of the hybrid film transits from light yellow for 8 nm Ag to orange for 8 nm Au/1LG/8 nm Ag, originating from the strong reflection of yellow light or red light. Apart from the shift of the resonant wavelength, the increase in the absorption is considered to be caused by the enhanced coupling in the graphene-plasmonic hybrid systems with enhanced light-matter interactions.[27,36]

Numerical simulations based on the finite element method (FEM) were performed to investigate the coupling effects in Au NP–graphene–Ag NP hybrids. As shown in Fig. 2c, a layer of 1 nm-thick graphene was sandwiched between vertically stacking Au and Ag NPs with a diameter of 48 nm (mimicking the 8 nm Ag or Au) in the simulations. Fig. 2d shows the simulated electrical field intensity distributions in the *xz* plane. It can be clearly seen that the localized electric field is mainly distributed at the gaps formed between horizontal Au or Ag NPs or between vertical Au/Ag NPs. Especially, the electric field has been strongly enhanced at the interface where graphene acts as a sub-nanometer dielectric gap, leading to a maximal enhancement of 87 (the maximal electric field enhancement is 3.9 or 8.5 for horizontal Au/Au or Ag/Ag NPs, respectively). Thus, a multi-dimensional coupling system including the plasmonic coupling on both horizontal and vertical directions has been established in such an Au–graphene–Ag hybrid structure.

As a result of the strongly enhanced electric field in the hybrid system, the SERS signals have been largely enhanced, as illustrated in Fig. 3a. For comparison, the Raman spectra of RhB with the same concentration on quartz, 8 nm Ag and 8 nm Au/8 nm Ag films, were also measured and are shown in the figure. The excitation of surface plasmons has led to much stronger Raman signals on metal NPs substrates than those on quartz, and all typical vibrational modes are observed. In detail, the 1359, 1506 and 1649 cm^{-1} peaks are attributed to aromatic C–C stretching; 1281 cm^{-1} to aromatic C–C bridge-band stretching, 1200 cm^{-1} to aromatic C–H bending and 622 cm^{-1} to aromatic bending.[10] Compared to the case of 8 nm Ag, the Raman signals of RhB (based on 1649 cm^{-1}) were enhanced about 2 times on 8 nm Au/8 nm Ag and 5 times on 8 nm Au/1LG/8 nm Ag films, respectively. A similar phenomenon was also obtained for R6G molecules (Fig. S5a, ESI†). The large enhancement in Raman signals for Au–graphene–Ag hybrids can be attributed to the wide range of hot spots with intensely enhanced electric field and the unique structure of the sandwiched structure that was optimized to match the excitation laser wavelength.[32,40] In addition, the chemical enhancement of graphene due to the π–π interactions and charge transfer between graphene and aromatic RhB and R6G molecules may also benefit the Raman enhancement.[9,26]

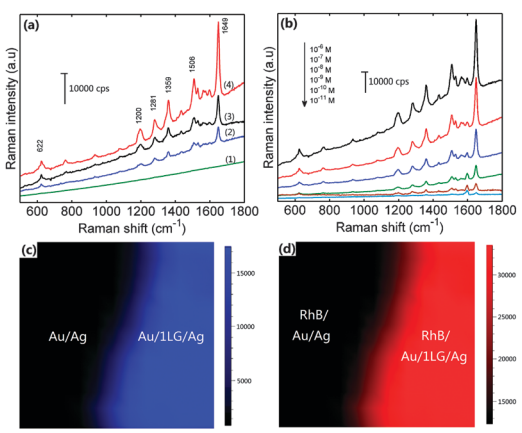

Fig. 3 (a) Raman spectra of 10^{-7} M RhB on quartz (curve 1), 8 nm Ag (curve 2), 8 nm Au/8 nm Ag (curve 3) and 8 nm Au/1LG/8 nm Ag (curve 4), respectively. (b) SERS spectra of RhB on the 8 nm Au/1LG/8 nm Ag structure with 6 different molecular concentrations. Spatially resolved Raman intensity mapping of (c) G peak of graphene at 1597 cm^{-1} before depositing RhB and (d) 10^{-7} M RhB at 1649 cm^{-1} on both 8 nm Au/8 nm Ag (left region) and 8 nm Au/1LG/8 nm Ag films (right region).

The SERS spectra of RhB deposited on the 8 nm Au/1LG/8 nm Ag hybrid structure at various molecular concentrations are shown in Fig. 3b and the intensity *versus* concentration curve is shown in Fig. S6, ESI.† The Raman signals are still observable even when the concentration is decreased to a value as low as 0.01 nM. The detection limit of 0.01 nM was also obtained from R6G (Fig. S5b, ESI†) and TNT (Fig. S7a, ESI†) on a hybrid substrate. By comparing the Raman spectra of RhB, R6G and TNT (Fig. S7b and S8, ESI†) on quartz substrates, the EFs obtained from the 8 nm Au/1LG/8 nm Ag films are 2.3×10^9 for RhB, 1.7×10^9 for R6G and 3.8×10^9 for TNT, respectively.

The spatially resolved Raman intensity mapping is used to demonstrate the high sensitivity and uniformity of Au NP–graphene–Ag NP hybrid films. Fig. 3d shows the mapping images of RhB at 1649 cm^{-1} in the area of 10×10 μm^2 for 8 nm Au/8 nm Ag film (left region) and 8 nm Au/1LG/8 nm Ag film (right region). It can be seen that the SERS intensity mapping of RhB is highly consistent with the G peak mapping of graphene that was measured before depositing RhB, as shown in Fig. 3c. This agreement suggests that the presence of graphene is essential to the enhanced SERS sensitivity of RhB molecules. At the same time, the graphene embedded area shows highly homogeneous adsorption for RhB molecules,[36] further demonstrating the reproducibility of Raman signals. We also measured the Raman signals on the same 8 nm Au/1LG/8 nm Ag films after it was kept in our lab for two months. The Raman intensity showed a decrease of 4% for RhB and 2% for R6G (Fig. S9, ESI†), indicating that the hybrid films fabricated by the simple and cost-effective preparation can maintain the Raman activity for a long time.

In addition, we found that the Raman enhancement of RhB on the Au NP–graphene–Ag NP hybrid system can be further increased by replacing the quartz substrate with a metal film-covered quartz substrate due to the hybridization between the localized surface plasmons (LSP) of metallic NPs and propagating surface plasmon polaritons (SPP) on the metal film.[4,5,7,25] Compared to the Raman signals of RhB on the 8 nm Au/1LG/8 nm Ag/quartz substrate with the same molecule concentration, the Raman intensity is further improved about 7 times at 1649 cm^{-1} after setting the sandwiched structure on a 100 nm-thick Ag film-covered quartz substrate, as shown in Fig. 4a. FEM simulated results (Fig. 4b, inset) show an additional SPP mode between the Ag NPs and the Ag film on quartz, leading to the further coupling of the LSP modes (between horizontal and vertical gaps of Au and Ag NPs) and the SPP mode (the maximal electric field enhancement is 115 or 87 at the graphene-defined gap

 This journal is © The Royal Society of Chemistry 2015

Published on 18 November 2014. Downloaded by University of Science and Technology of China on 10/03/2016 03:24:25.

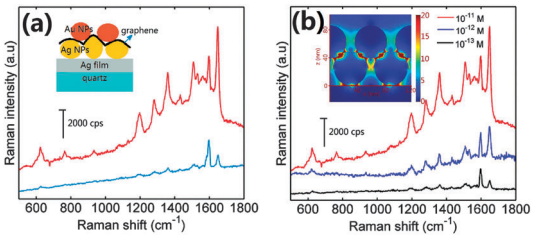

Fig. 4 (a) Raman spectra of 10^{-11} M RhB on the 8 nm Au/1LG/8 nm Ag/100 nm-thick Ag film/quartz substrate (upper curves) and 8 nm Au/1LG/8 nm Ag/quartz (bottom curves). The inset shows the schematic diagram of the Au NP–graphene–Ag NP–Ag film/quartz structure. (b) Raman spectra of RhB on the 8 nm Au/1LG/8 nm Ag/Ag film/quartz structure with molecular concentration varying from 10^{-11} M to 10^{-13} M. The inset shows the simulated electrical field intensity distributions of Au NP–graphene–Ag NP on an Ag substrate in the *xz* plane with $y = 24$ nm. The color bar indicates the magnitude of the electric field normalized by the incident field.

for the hybrid system on Ag film or a quartz substrate, respectively), *i.e.*, further enhanced multi-dimensional coupling.[25] The Raman signals of RhB can be clearly visible down to 10^{-13} M (Fig. 4b), demonstrating the ultrasensitive detection capability of the SERS substrate based on the graphene embedded metal NP hybrid structure on metal Ag films. Such a detection capability is not achievable with typical Au nanosphere on Ag films[7] or Au NP/Ag NP on Ag films (Fig. S10, ESI†). As far as we know, the detection limit of 10^{-13} M is the lowest value using a metal nanosphere (or similar to a nanosphere) on metal films.[5,40,41]

In conclusion, we have developed an efficient SERS substrate by utilizing the multi-dimensional plasmonic coupling in Au NP–graphene–Ag NP hybrid structures. The plasmonic resonant wavelength of the hybrid platform can be readily tuned by the thickness of Au or Ag films deposited; an 8 nm Au/1LG/8 nm Ag structure has achieved a resonant wavelength equal to the excitation laser wavelength (532 nm). Finite element numerical simulations were used to identify the coupling between horizontal and vertical Au/Ag NPs, leading to a strong electric field enhancement. The Au NP–graphene–Ag NP structures on quartz have demonstrated SERS EFs of over 10^9 for RhB, R6G and TNT. Moreover, an ultrasensitive SERS detection with a limit down to 10^{-13} M can be achieved when the hybrid film is fabricated on the Ag substrate instead of quartz due to the hybridization between LSP of metal NPs and SPP of Ag film. The proposed SERS systems may find promising applications in areas of analytical chemistry, biomedical diagnostics, biological sensing and imaging.

This work was supported by China Government 1000 Plan Talent Program, China MOE NCET Program, NSFC Program (51322204) and the Fundamental Research Funds for the Central Universities (WK2060140014).

Notes and references

1 M. Fleischmann, P. J. Hendra and A. J. Mcquillan, *Chem. Phys. Lett.*, 1974, **26**, 163–166.
2 A. Campion and P. Kambhampati, *Chem. Soc. Rev.*, 1998, **27**, 241–250.
3 W. Xu, N. Mao and J. Zhang, *Small*, 2013, **9**, 1206–1224.
4 M. Rycenga, X. Xia, C. H. Moran, F. Zhou, D. Qin, Z.-Y. Li and Y. Xia, *Angew. Chem., Int. Ed.*, 2011, **50**, 5473–5477.
5 L. Li, T. Hutter, U. Steiner and S. Mahajan, *Analyst*, 2013, **138**, 4574–4578.
6 X. Xia, J. Zeng, B. McDearmon, Y. Zheng, Q. Li and Y. Xia, *Angew. Chem., Int. Ed.*, 2011, **50**, 12542–12546.
7 J. Lee, B. Hua, S. Park, M. Ha, Y. Lee, Z. Fan and H. Ko, *Nanoscale*, 2014, **6**, 616–623.
8 A. Tao, F. Kim, C. Hess, J. Goldberger, R. R. He, Y. G. Sun, Y. N. Xia and P. D. Yang, *Nano Lett.*, 2003, **3**, 1229–1233.
9 P. Wang, O. Liang, W. Zhang, T. Schroeder and Y.-H. Xie, *Adv. Mater.*, 2013, **25**, 4918–4924.
10 A. Liu, T. Xu, J. Tang, H. Wu, T. Zhao and W. Tang, *Electrochim. Acta*, 2014, **119**, 43–48.
11 Y. Han, R. Lupitskyy, T.-M. Chou, C. M. Stafford, H. Du and S. Sukhishvili, *Anal. Chem.*, 2011, **83**, 5873–5880.
12 J. C. Reed, H. Zhu, A. Y. Zhu, C. Li and E. Cubukcu, *Nano Lett.*, 2012, **12**, 4090–4094.
13 P. P. Patra and G. V. P. Kumar, *J. Phys. Chem. Lett.*, 2013, **4**, 1167–1171.
14 Z. Xia, C. Yanhua, C. Yang, B. Ning, Q. Haibo, Q. Meihong, S. Dan, Z. Hanqi and T. Yuan, *J. Raman Spectrosc.*, 2012, **43**, 1374–1380.
15 J. F. Li, Y. F. Huang, Y. Ding, Z. L. Yang, S. B. Li, X. S. Zhou, F. R. Fan, W. Zhang, Z. Y. Zhou, D. Y. Wu, B. Ren, Z. L. Wang and Z. Q. Tian, *Nature*, 2010, **464**, 392–395.
16 T. Hirakawa and P. V. Kamat, *J. Am. Chem. Soc.*, 2005, **127**, 3928–3934.
17 D. Wang, W. Zhu, M. D. Best, J. P. Camden and K. B. Crozier, *Sci. Rep.*, 2013, **3**, 2867.
18 X. Li, J. Li, X. Zhou, Y. Ma, Z. Zheng, X. Duan and Y. Qu, *Carbon*, 2014, **66**, 713–719.
19 W. L. Barnes, A. Dereux and T. W. Ebbesen, *Nature*, 2003, **424**, 824–830.
20 G. Xu, J. Liu, Q. Wang, R. Hui, Z. Chen, V. A. Maroni and J. Wu, *Adv. Opt. Mater.*, 2012, **24**, OP71–OP76.
21 V. G. Kravets, F. Schedin, R. Jalil, L. Britnell, K. S. Novoselov and A. N. Grigorenko, *J. Phys. Chem. C*, 2012, **116**, 3882–3887.
22 W. Xu, X. Ling, J. Xiao, M. S. Dresselhaus, J. Kong, H. Xu, Z. Liu and J. Zhang, *Proc. Natl. Acad. Sci. U. S. A.*, 2012, **109**, 9281–9286.
23 W. Xu, J. Xiao, Y. Chen, Y. Chen, X. Ling and J. Zhang, *Adv. Mater.*, 2013, **25**, 928–933.
24 W. Fan, Y. H. Lee, S. Pedireddy, Q. Zhang, T. Liu and X. Y. Ling, *Nanoscale*, 2014, **6**, 4843–4851.
25 X. Li, W. C. H. Choy, X. Ren, D. Zhang and H. Lu, *Adv. Funct. Mater.*, 2014, **24**, 3114–3122.
26 X. Ling, L. Xie, Y. Fang, H. Xu, H. Zhang, J. Kong, M. S. Dresselhaus, J. Zhang and Z. Liu, *Nano Lett.*, 2010, **10**, 553–561.
27 X. Zhu, L. Shi, M. S. Schmidt, A. Boisen, O. Hansen, J. Zi, S. Xiao and N. A. Mortensen, *Nano Lett.*, 2013, **13**, 4690–4696.
28 Q. Hao, B. Wang, J. A. Bossard, B. Kiraly, Y. Zeng, I. K. Chiang, L. Jensen, D. H. Werner and T. J. Huang, *J. Phys. Chem. C*, 2012, **116**, 7249–7254.
29 H. Zhou, C. Qiu, Z. Liu, H. Yang, L. Hu, J. Liu, H. Yang, C. Gu and L. Sun, *J. Am. Chem. Soc.*, 2010, **132**, 944–946.
30 C. Qiu, H. Zhou, B. Cao, L. Sun and T. Yu, *Carbon*, 2013, **59**, 487–494.
31 A. P. Liu, T. Xu, Q. H. Ren, M. Yuan, W. J. Dong and W. H. Tang, *Electrochem. Commun.*, 2012, **25**, 74–78.
32 L. Zhang, C. Jiang and Z. Zhang, *Nanoscale*, 2013, **5**, 3773–3779.
33 Y. Zhao, X. Li, Y. Du, G. Chen, Y. Qu, J. Jiang and Y. Zhu, *Nanoscale*, 2014, **6**, 11112–11120.
34 Plasma Sputter Coating. http://www.mtixtl.com/desktopplasmasputtering-coaterformetalliccoatingwithvacuumpumpandgoldtarget15maxsample.aspx, MTI Corporation.
35 X. Li, W. Cai, J. An, S. Kim, J. Nah, D. Yang, R. Piner, A. Velamakanni, I. Jung, E. Tutuc, S. K. Banerjee, L. Colombo and R. S. Ruoff, *Science*, 2009, **324**, 1312–1314.
36 Y. Du, Y. Zhao, Y. Qu, C.-H. Chen, C.-M. Chen, C.-H. Chuang and Y. Zhu, *J. Mater. Chem. C*, 2014, **2**, 4683–4691.
37 J. Lee, S. Shim, B. Kim and H. S. Shin, *Chem. – Eur. J.*, 2011, **17**, 2381–2387.
38 G. Fan, H. Zhu, K. Wang, J. Wei, X. Li, Q. Shu, N. Guo and D. Wu, *ACS Appl. Mater. Interfaces*, 2011, **3**, 721–725.
39 G. Lu, H. Li, C. Liusman, Z. Yin, S. Wu and H. Zhang, *Chem. Sci.*, 2011, **2**, 1817–1821.
40 H.-J. Ahn, P. Thiyagarajan, L. Jia, S.-I. Kim, J.-C. Yoon, E. L. Thomas and J.-H. Jang, *Nanoscale*, 2013, **5**, 1836–1842.
41 S. Wang, L.-P. Xu, Y. Wen, H. Du, S. Wang and X. Zhang, *Nanoscale*, 2013, **5**, 4284–4290.